Radiation-induced modifications in structural, electrical and dielectric properties of Ti^{4+} ions substituted $Li_{0.5}Fe_{2.5}O_4$ nanoparticles

Published: 13 March 2018

Volume 29, pages 8601–8609, (2018) Cite this article

Journal of Materials Science: Materials in Electronics

Aims and scope

Submit manuscript

Jitendra S. Kounsalye, Prashant B. Kharat, Dhananjay N. Bhoyar & K. M. Jadhav

Abstract

In the present study, $Li_{0.5+0.5x}Ti_xFe_{2.5-1.5x}O_4$ (where, $0.0 \leq x \leq 1.0$ in step of 0.2) nanoparticles were synthesized via sol–gel auto combustion technique. The nanocrystalline samples exposed to ^{60}Co gamma (γ)-radiation of 5 Mrad dose, to understand its effect on structural,

morphological, electrical and dielectric properties. The nanoparticles characterized by X-ray diffraction and field emission scanning electron microscopy (FE-SEM) techniques before and after irradiation. The irradiated samples give good crystallinity, and small crystallite size (~ 25 nm) as compared to pristine samples (~ 45 nm) and the lattice parameter gets decreased up to ~ 0.01 Å. The FE-SEM images of pristine samples show spherical morphology, whereas irradiated samples showed some cracks in it. Temperature-dependent conductivity measured by two probe technique reveals that the conductivity decreases (upto ~ $5 \times 10^{-5} \Omega^{-1}$) after irradiation by obeying Ohmic nature. The dielectric measurements show the strong influence of irradiation on all the samples.

1 Introduction

The combined electric and magnetic properties of spinel ferrites make them unique as well as applicable in many fields such as transformer core, recording media, biomedical, a cathode material for Li-ion battery, supercapacitor, etc. [1]. They are convenient for both electronic

and magnetic applications [2]. Lithium ferrite (Li-ferrite) is a cubic spinel ferrite, which belongs to the family of soft ferrite materials with a square hysteresis loop. They possess high Curie temperature (~ 900 K [3]) and high saturation magnetization (~ 60 emu/gm [4]) thus it is applicable in the microwave and high-frequency devices. The cubic spinel structure of Li-ferrite has two crystalline forms, namely ordered α-phase with $P4_132/P4_332$ space group and disordered β-phase with Fd-3m space group [5, 6]. Li-ferrites can be useful for various technological applications like microwave devices, computer memory chip, magnetic recording, radio frequency coil fabrication, transformer cores, rod antennas, magnetic liquids [7,8,9], etc. Li-ferrite and substituted Li-ferrites are also a capable nominee for cathode material in lithium batteries [10].

The properties of Li-ferrites are sensitive to various aspects such as the method of preparation [11], synthesis parameters [12], substituted cations [13], annealing temperature [14]. In literature, various techniques applied for the synthesis of spinel ferrite in a nanocrystalline form [15]. Among the several methods, sol–gel auto combustion technique has many advantages such as homogeneity, uniform grains, small crystallite size, requires low temperature and cost-effective [16, 17], etc. The properties of Li-ferrite modified by exposing it to different radiations like X-rays and gamma rays etc. [18, 19]. Moreover, high dose of γ-radiation may create many defects in the crystal hence, the study of γ-radiation effects in Li-ferrite is essential for their role in industrial applications. The amount of defect formation and property alteration strongly depends on the type of radiation and dose of radiation etc. The high-energy irradiation may create an interesting phenomenon like sputtering of target materials, surface morphological changes, etc. Ionizing radiation produces a large number of ionized and excited molecules along its path. Also, they are non-selective and may interact with any particle in its pathway. Substitution of the Ti^{4+} increases high-frequency response of spinel ferrites, even in recent year's application of lithium ferrite enlarged significantly because of Gigahertz range applications at present. The addition of titanium yield dilute spin glass behavior in lithium ferrites and can enhance the frequency range [20, 21].

The introduction of Ti^{4+} ions in the Li-ferrite as well as the γ-rays reduces the formation of Fe^{2+} ions and creates some defects. Thus, γ-radiation and substitution of Ti^{4+} ion can modify structural, morphological, electric and dielectric properties of Li-ferrite. In literature, the γ-radiation effect on spinel ferrite was studied by many researchers [22,23,24,25,26] and they

found the properties of Li-ferrite are susceptible to the radiation and these properties can be modified using an appropriate dose.

With this view, in the existing study, we are projected to investigate the influence of (5 Mrad) γ-radiation on structural, morphological, electrical and dielectric properties of Ti^{4+} substituted Li-ferrite nanoparticles synthesized via sol–gel auto combustion technique.

2 Experimental

2.1 Synthesis of $Li_{0.5+0.5x}Ti_xFe_{2.5-1.5x}O_4$ nanoparticles

Lithium nitrate ($LiNO_3$), ferric nitrate nonahydrate ($Fe(NO_3)_3{\cdot}9H_2O$), tetra butyl titanate ($C_{16}H_{36}O_4Ti$) as a source of Li^+, Fe^{3+}, and Ti^{4+} ions respectively. And citric acid ($C_6H_8O_7$) as a fuel, distilled water (DH_2O) and ethanol (C_2H_6O) as a solvent were used for the synthesis. All the chemicals of AR grade with ~ 99.99% purity were purchased from Sigma-Aldrich (Merck) and used for synthesis without further purification. Using sol–gel auto-combustion technique the $Li_{0.5+0.5x}Ti_xFe_{2.5-1.5x}O_4$ system with $0.0 \leq x \leq 1.0$ in step of 0.2 were prepared. In our previous work, the details of synthesis procedure are reported [27]. The as-synthesized powder was annealed at 800 °C for 6 h for removing an impurity of nitrate remained, also for well crystal growth.

Two sets of the annealed samples were prepared, out of which one set of samples was subjected to the planned exposure of Co^{60} gamma radiation using gamma chamber, with a dose rate of 0.1 Mrad/h. The total dose time estimated for irradiation was 50 h to complete the entire dose of 5 Mrad.

2.2 Characterizations

The XRD patterns were recorded on Rigaku (Miniflex-2) diffractometer using CuK_α (λ = 1.541 Å) radiation in the 2θ range of 20°–80°. The Hitachi (S-4800), field emission scanning electron microscope was used to study the morphology of representative samples. The temperature dependence of DC conductivity was measured using two probe technique in the temperature range of 700–1000 K in step of 10 K, I–V characteristics were studied using the Keithely source meter (2400), in the range from + 5 to − 5 V to estimated room temperature

resistivity. The dielectric properties were examined using the LCR-Q meter in the frequency range of 50 Hz to 5 MHz.

3 Results and discussion

3.1 Structural properties

The Figs. 1, 2, 3, 4, 5 and 6 shows XRD patterns for pristine and γ-irradiated samples of $Li_{0.5+0.5x}Ti_xFe_{2.5-1.5x}O_4$ nanoparticles. The XRD patterns of LTF-1 sample well matches with JCPDS card # 82-1436 which belongs to $P4_132/P4_332$ space group; corresponds to ordered (α) phase. The remaining XRD patterns for LTF-2-6 samples well match with JCPDS card # 74-1911 which belongs to Fd-3m space group; corresponds to disordered (β) phases. The XRD patterns revealed the reflections about cubic spinel structure; no impurity peaks have been observed in the XRD pattern for LTF-1 to four samples. However, in XRD patterns of LTF-5,6 samples, some reflections belong to TiO_2, and $Li_2[O_2]$ phases were oriented, which may attribute to the incomplete reaction during combustion. Also, higher substitution of Ti^{4+} ions at the place of Fe^{3+} ions having ionic radii 0.76 and 0.645 Å [28] respectively. Since, at higher concentration the Li^{1+}, Ti^{4+} ions are not adequately replacing the Fe^{3+} ions situated at octahedral [B] site. Thus the impurity phase was oriented. The γ-irradiated XRD patterns high intensity and have broader peak shape, which confirms that the γ-irradiated samples are more crystalline with small crystallite size as compared with pristine samples [29]. In the irradiated samples; due to the incident radiation some color centers are formed in the crystal, and we found suitable crystalline material. Also, the massive difference in intensity can attribute to change in atomic form factor due to ionization of atoms after γ-irradiation. Moreover, the micro stress generated by defects due to gamma irradiation leads to broadening of diffraction peaks simultaneously.

Fig. 1

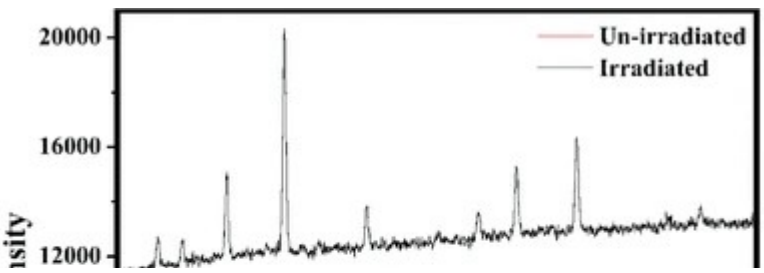

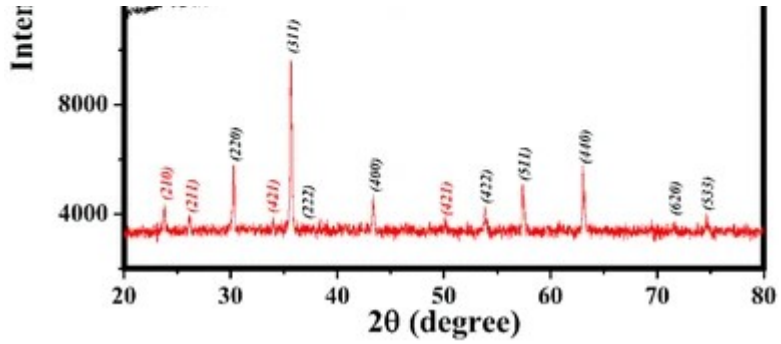

X-ray diffraction pattern of γ-irradiated and unirradiated samples of LTF-1 nanoparticles. (Color figure online)

Fig. 2

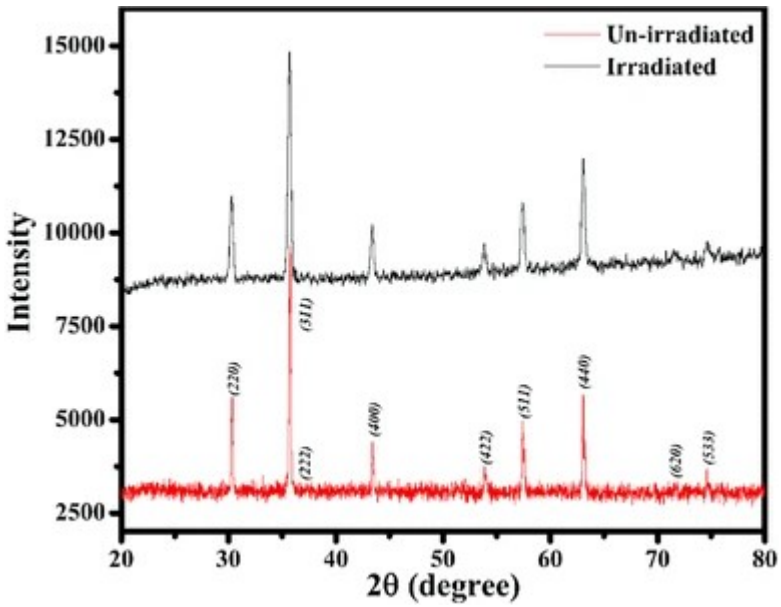

X-ray diffraction pattern of γ-irradiated and unirradiated samples of LTF-2 nanoparticles. (Color figure online)

Fig. 3

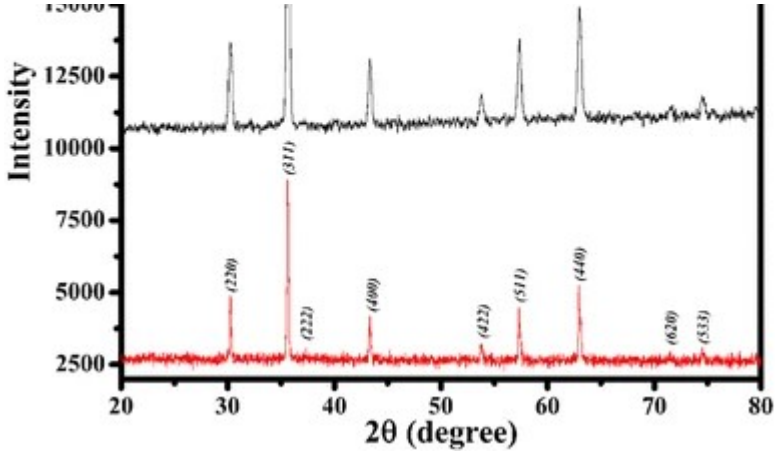

X-ray diffraction pattern of γ-irradiated and unirradiated samples of LTF-3 nanoparticles. (Color figure online)

Fig. 4

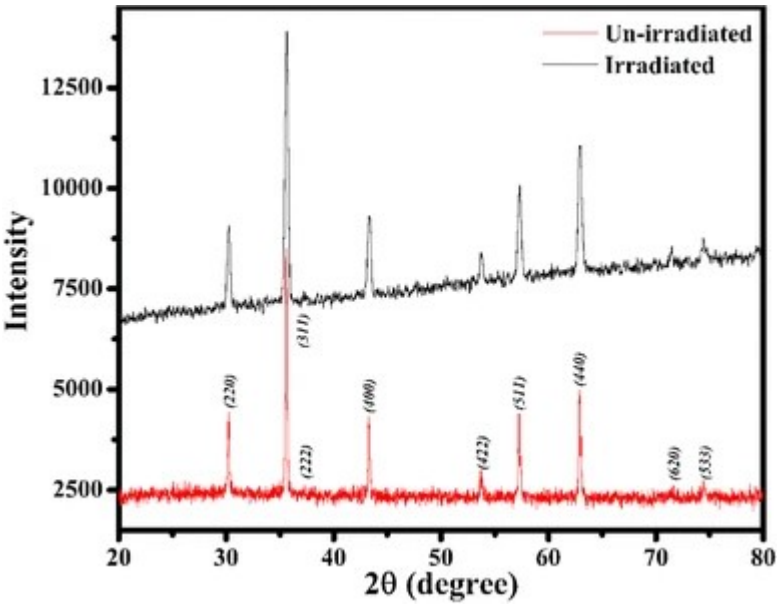

X-ray diffraction pattern of γ-irradiated and unirradiated samples of LTF-4 nanoparticles. (Color figure online)

Fig. 5

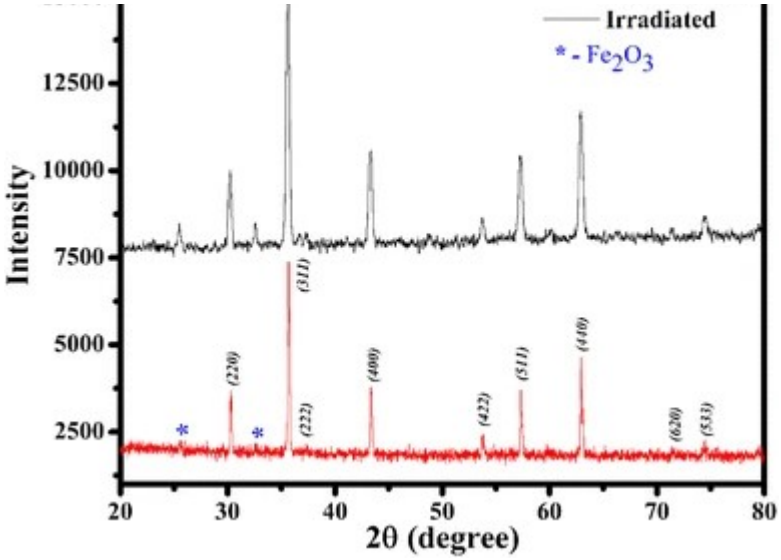

X-ray diffraction pattern of γ-irradiated and unirradiated samples of LTF-5 nanoparticles. (Color figure online)

Fig. 6

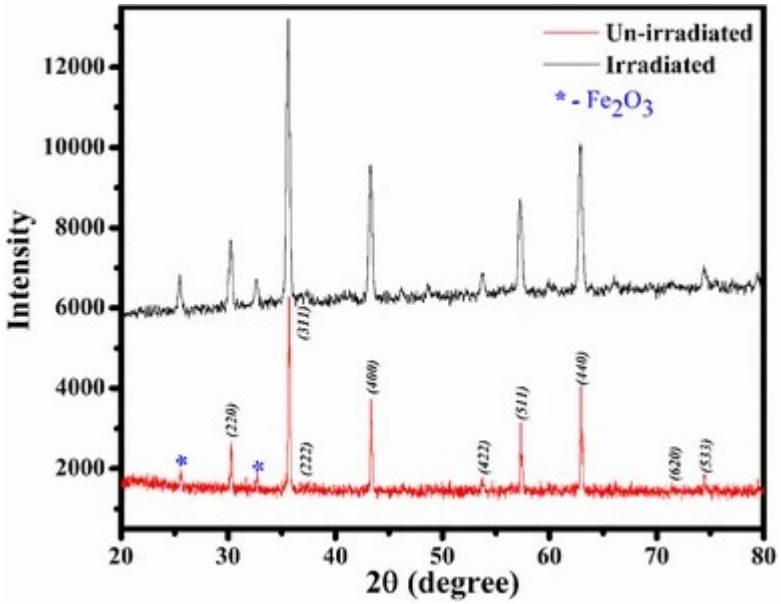

X-ray diffraction pattern of γ-irradiated and unirradiated samples of LTF-6 nanoparticles. (Color figure online)

The lattice parameter (a) was calculated using standard relation [30] with the error of ± 0.001,

and the values are listed in Table 1. The obtained values of the lattice parameter are compatible with JCPDS data. However, it is evident from Table 1 that the lattice parameter decreases after irradiation. And the lattice parameter found to increase with an increase in Ti^{4+} concentration x after irradiation. The difference in ionic radii of Ti^{4+} (0.76 Å) and Fe^{3+} (0.645 Å) ion leads to increase in lattice parameter. The variation of lattice parameter with Ti^{4+} ion concentration is shown in Fig. 7. From Fig. 7 it is clear that for irradiated samples the difference in lattice parameter as a function of Ti^{4+} concentration follow the similar trend as that of pristine samples. The incident radiations increase the energy of ions situated at lattice sites, and hence, it results in a decrease in lattice parameter and increases in density of the crystal after irradiation. The X-ray density (d_x) [31] was also estimated and summarized in Table 1; the values decreased with increasing Ti^{4+} concentration x which is due to fall in molecular mass. For irradiated samples holds slightly higher values, the increase in X-ray density for irradiated samples attribute to the rise in agglomeration of atoms after irradiation.

Table 1 Lattice parameter (a), X-ray density (d_x), hopping length (L_A, L_B), tetrahedral bond (d_{AL}), octahedral bond (d_{BL}), tetra edge (d_{AE}) and octa edge (d_{BEU}) shared and unshared of $Li_{0.5+0.5x}Ti_xFe_{2.5-1.5x}O_4$ nanoparticles

Fig. 7

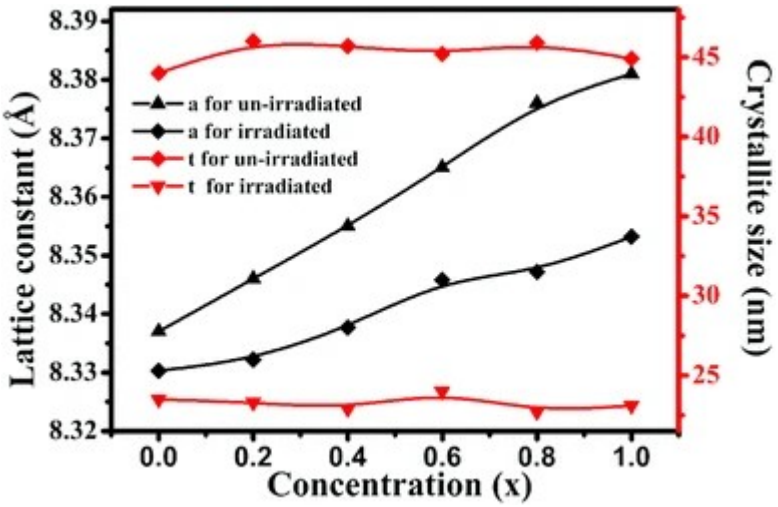

Variation of lattice constant and crystallite size with concentration for γ-irradiated and unirradiated $Li_{0.5+0.5x}Ti_xFe_{2.5-1.5x}O_4$ nanoparticles. (Color figure online)

The intensity of (311) plane is more than that of other planes. Thus the crystallite size was calculated using FWHM of (311) peak by Scherrer's formula [32] and tabulated in Table 2. The values show nanocrystalline nature of the present system before and after irradiation. It can be seen from Fig. 7 that the crystallite size drastically changed after irradiation, which is due to increase in agglomeration of atoms by irradiation like quenching process. Similar observations are also found in the literature for Ni–Zn ferrite [24], Co–Zn ferrite [23] after gamma irradiation. The small particle size leads to many nanotechnological applications [33, 34]. Hence the irradiated samples can be more useful for many technological applications as compared with the pristine samples.

Table 2 Ionic radii (r_A, r_B) of tetrahedral and octahedral site and average crystallite size (t) of pristine (before) and γ-irradiated (after) $Li_{0.5+0.5x}Ti_xFe_{2.5-1.5x}O_4$ nanoparticles and grain size (G) for typical samples and porosity

The structural parameters, i.e., hopping lengths (L_A, L_B), tetrahedral bond length (d_{AL}),

octahedral bond length (d_{BL}), tetra edge (d_{AE}) and octa edge (d_{BEU}) were also determined for all pristine and irradiated samples using the standard relations [35, 36]. The variation of all these structural parameters with Ti^{4+} content x is similar to the behavior of lattice parameter (a) with x as well as with γ-irradiation since all the parameters are proportional to the 'a'. The calculated values are listed in Table 2. The tetrahedral (A)-site ionic radii and octahedral [B]-site ionic radii [37] were also estimated using standard relations [38]. The values of the ionic radii are given in Table 2, and it is found that the ionic radii increase with an increase in Ti^{4+} concentration x. All the results are in good agreement with the previous report for gamma irradiated Li-ferrite [19].

3.2 FE-SEM analysis

FE-SEM images of typical samples of the present system are presented in Fig. 8 for pristine and irradiated samples respectively. The figures show that the fine spherical particles are agglomerated together. The porous space in agglomerated mobs can be credited to the release of gases during the combustion process of synthesis. After γ-irradiation, the cracked morphology was observed, which may be due to increase in surface energy by the energy released by the radiations at the surface during scattering. It is clear from Fig. 8 that the irradiation can damage the surface morphology of the sample. The average grain size was estimated using linear intercept method and found in the nanometer range which evidence that the nano size of the grains. The values of grain size are tabulated in Table 2. The decrease in grain size can be attributed to cracks in the grains after irradiation.

Fig. 8

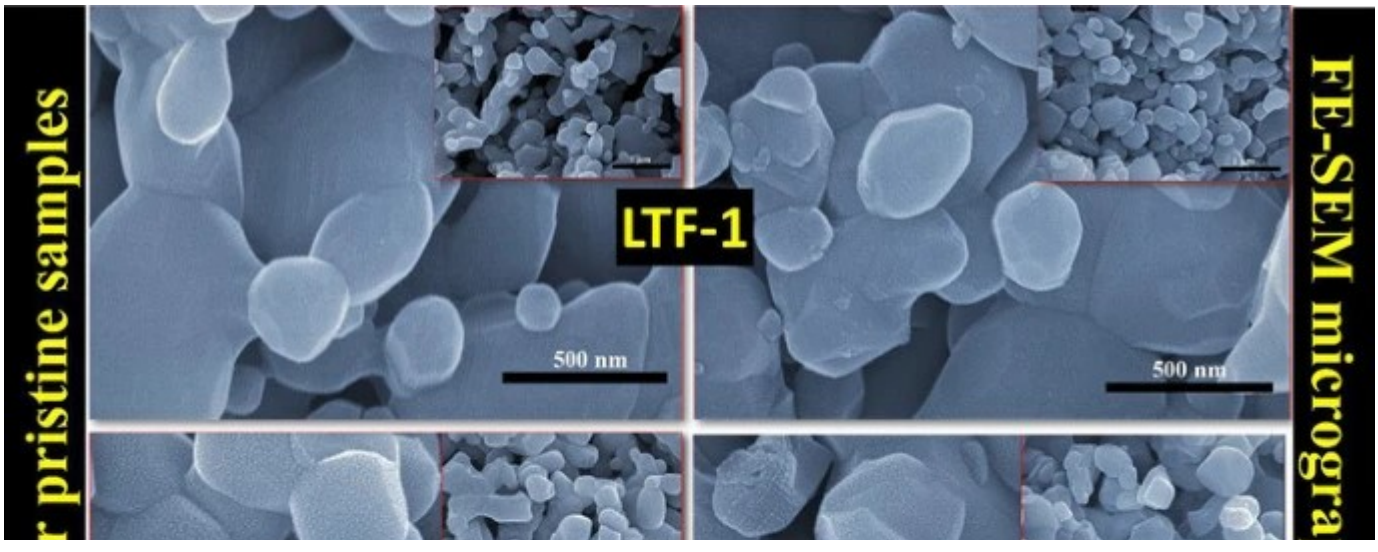

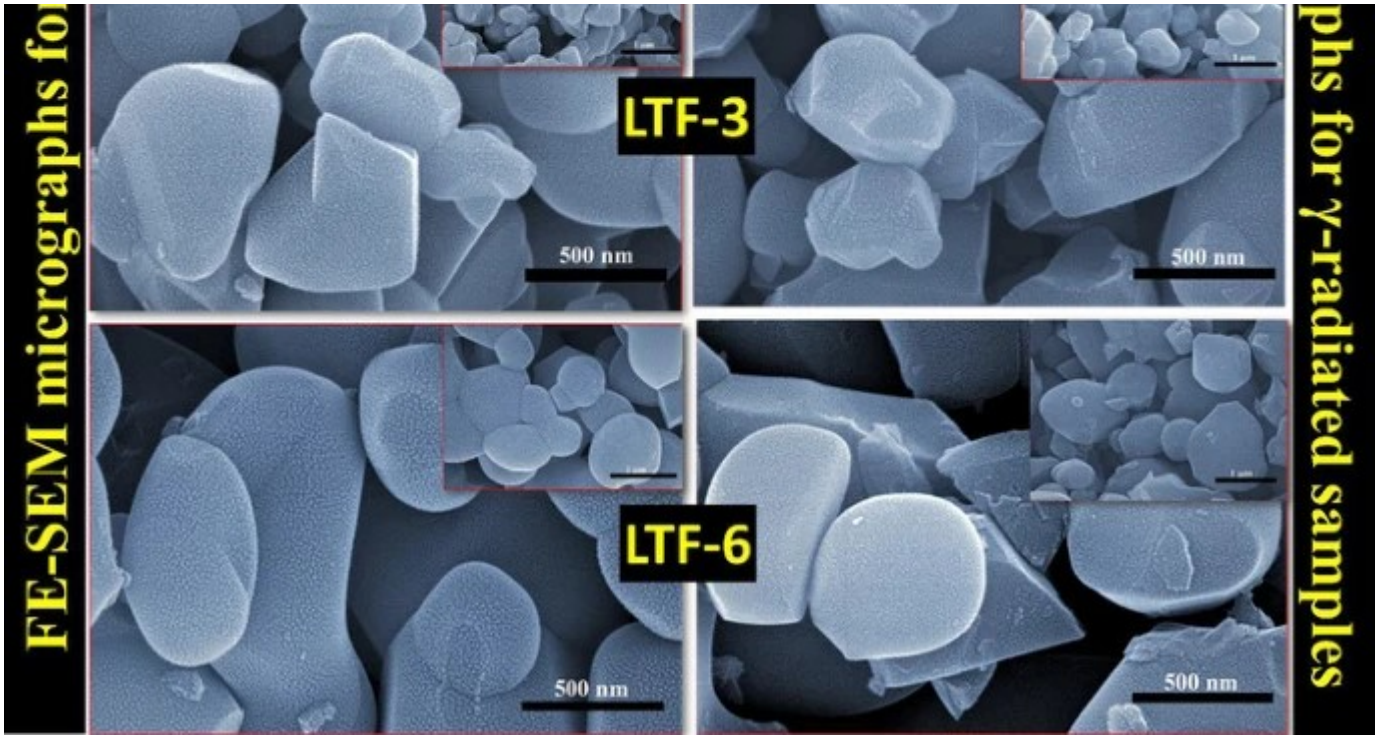

FE-SEM images of typical (LTF-1, 3, 6) un-irradiated and γ-irradiated $Li_{0.5+0.5x}Ti_xFe_{2.5-1.5x}O_4$ nanoparticles (scale in inset is 1μ m)

3.3 Electrical properties

The variation of electrical conductivity with temperature is shown in Fig. 9 for pristine and γ-irradiated samples. The plots show two distinct regions with its own conduction mechanism and different activation energy. Similar observations are found for the spinel ferrite in the literature [39]. The first one belongs to an ordered region with ferrimagnetic phase and the second one is a disordered region belongs to the paramagnetic phase [40]. The plot shows a change in slope in each region which corresponds to the Curie point [41, 42]. The electrical conductivity increases with increase in temperature; it proposes that the sample obeys Arrhenius relation [43] by showing semiconducting behavior. The graphs with linear nature suggest us that the variations obeys Wilson's law and possess semiconducting behavior. It is found that the substitution Ti^{4+} ions results in decreasing the conductivity. The values of activation energies calculated by Arrhenius plots are summarized in Table 3. The values in the paramagnetic region are higher as compared to that of in the ferromagnetic region. Since below Curie temperature, the conduction and valence bands split, while above Curie temperature bands are degenerate. Thus, it is expected that the activation energy should

enhance and the activation energy in the paramagnetic region must be larger. The DC resistivity for irradiated samples is higher as compared with the pristine one, which is due to the electronic exchange between Fe^{3+} to Fe^{2+} during the irradiation process which affects the hopping process.

Fig. 9

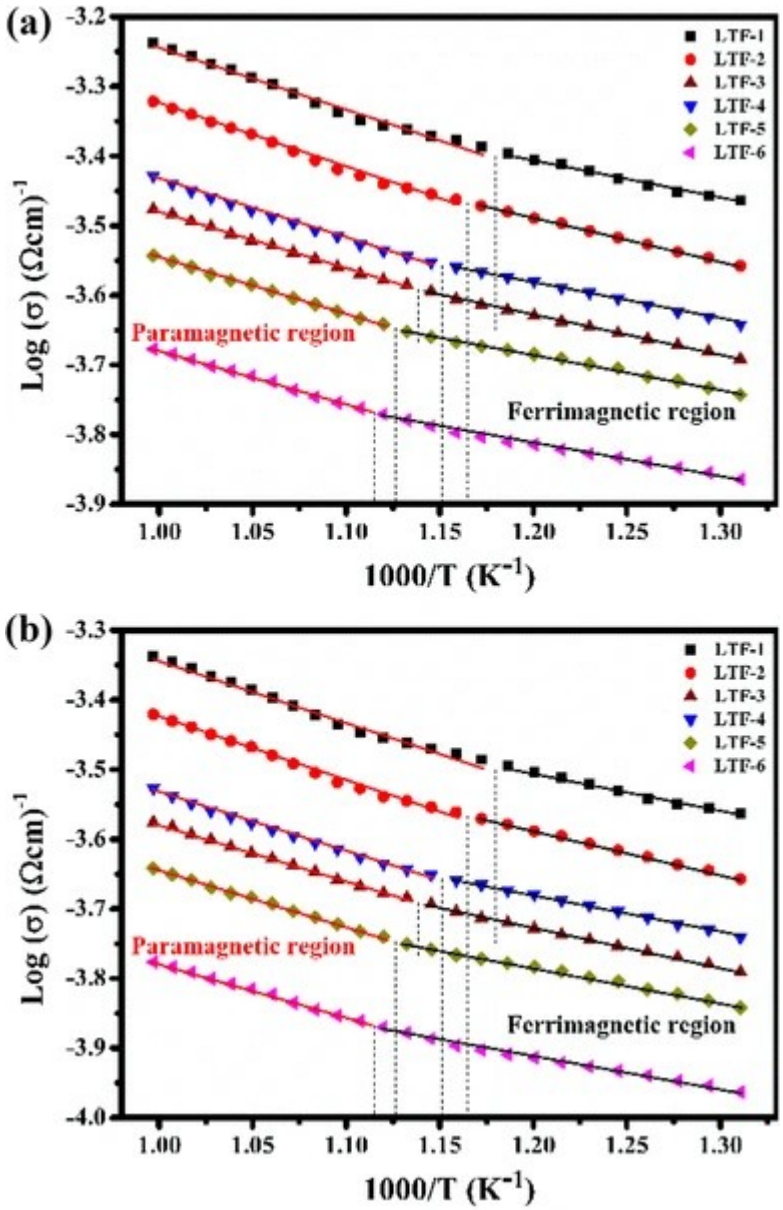

Variation of conductivity with reciprocal of temperature for a unirradiated and b γ-irradiated $Li_{0.5+0.5x}Ti_xFe_{2.5-1.5x}O_4$ nanoparticles (the marked line show Curie temperature)

Table 3 Activation energy of paramagnetic region (E_p) and ferromagnetic region (E_f), activation energy (ΔE) of pristine and γ-irradiated $Li_{0.5+0.5x}Ti_xFe_{2.5-1.5x}O_4$ nanoparticles and grain size (G) for typical samples

Since, the drift mobility of the charge carriers increases with temperature, the DC electrical resistivity decrease with temperature. The spinel ferrites possess the exponential dependence of DC electrical resistivity with temperature. In spinel ferrites, the charge carrier jumps from ion to ion, not through the crystal lattice and the conduction occurs due to the electronic exchange between Fe^{3+} to Fe^{2+}. Thus, the hopping mechanism can be used to explain conduction of spinel ferrite wherein charge carrier jumps from ion to ion. Further, the increase in conductivity with increase in temperature is related to the increase in lattice vibrations with temperature which in turn leads to more overlap of the orbital and therefore help the hopping mechanism. A similar variation is observed in case of the resistivity measured at room temperature. The room temperature DC resistivity of pristine and irradiated samples was represented in Fig. 10. The figure shows that the resistivity increases after irradiation for all the samples in the present series and the Ti^{4+} ions increases the resistivity of Li-ferrite. The electronic exchange, as well as the increase in the Fe^{2+}/Fe^{3+} ratio, may lead to increase in resistivity after irradiation [44]. The amount of impurity phases in LTF-6 samples is larger as in LTF-7 (Figs. 5, 6). Hence in this samples somewhat sudden decrease in DC conductivity, also after irradiation, the increase in impurity phase leads to over again fall in the DC conductivity value, these can clear from Fig. 9.

Fig. 10

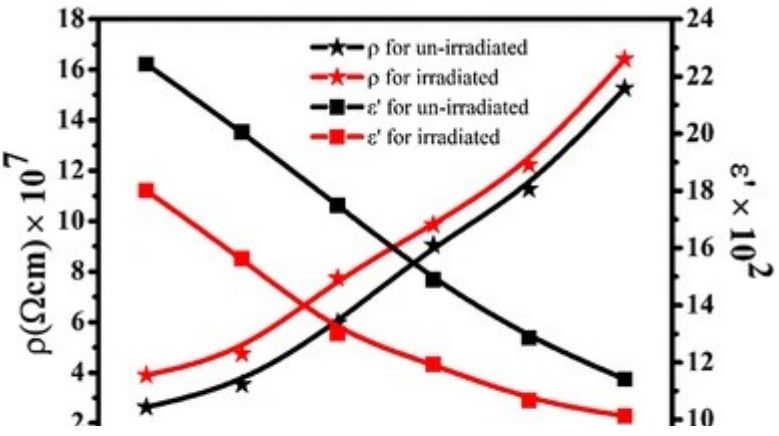

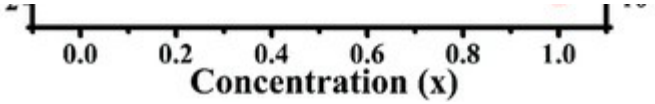

Room temperature resistivity and dielectric constant at 50 Hz frequency of γ-irradiated and unirradiated $Li_{0.5+0.5x}Ti_xFe_{2.5-1.5x}O_4$ nanoparticles. (Color figure online)

3.4 Dielectric properties

The dielectric properties of pristine and γ-irradiated samples were measured by LCR-Q meter at room temperature. The capacitance and loss tangent (tan δ) were measured in the frequency range of 50 Hz to 5 MHz. The dielectric constant (ε′) was estimated using standard relation [16], and the values of dielectric constant (ε′) and loss tangent (tan δ) are plotted against the log of frequency and presented in Figs. 11 and 12 respectively for pristine and γ-irradiated samples. These parameters decrease with Ti^{4+} ions substitution in Li-ferrite and also decreased after irradiation. The inverse relation of dielectric constant (at 50 Hz frequency) with resistivity for pristine and irradiated samples is shown in Fig. 10. The concept of conductivity in dielectric materials exhibits itself in a sketch of how lossy the dielectric material is, that how well the dielectric material converts the energy in the electric field at a certain frequency into heat. The figure shows that the dielectric constant decreased and the resistivity increased after irradiation. The electronic exchange during radiation process is responsible for decreases in dielectric constant after irradiation. The high value of dielectric constant at low frequency and rapidly decreases with increase in frequency is observed for all the samples. Since the dislocations, voids, and defects are present in the crystal structure of nano ferrites; at low frequencies cause the high value of dielectric constant. When the frequency reaches a certain frequency limit, the electron hopping cannot follow the electric field fluctuations and tends to decrease the dielectric constant with increasing frequency. The decreased behavior of dielectric constant with increasing frequency is because at higher frequencies; any effect is contributing to polarization is found to struggling. At high frequencies, the dielectric constant reaches less value due to high conductivity values and becomes less dependent on frequency. The variation of dielectric constant with frequency can be explained by space charge polarization due to an inhomogeneous dielectric structure as discussed by Maxwell and Wagner [45], also obeying Koops' theory [46]. As Ti^{4+} ions increase in Li-ferrite, the values of dielectric constant decrease, after irradiation, the values are

somewhat less with the same behavior with frequency. The defects produced by irradiation cause the change in dielectric properties after irradiation [47]. At low frequencies, the difference is more as compared to high frequencies. With decreasing Fe ions which are responsible for polarization, it is expected to decrease the dielectric constant for the present system. Similar results are available in the literature for spinel ferrites [48, 49].

Fig. 11

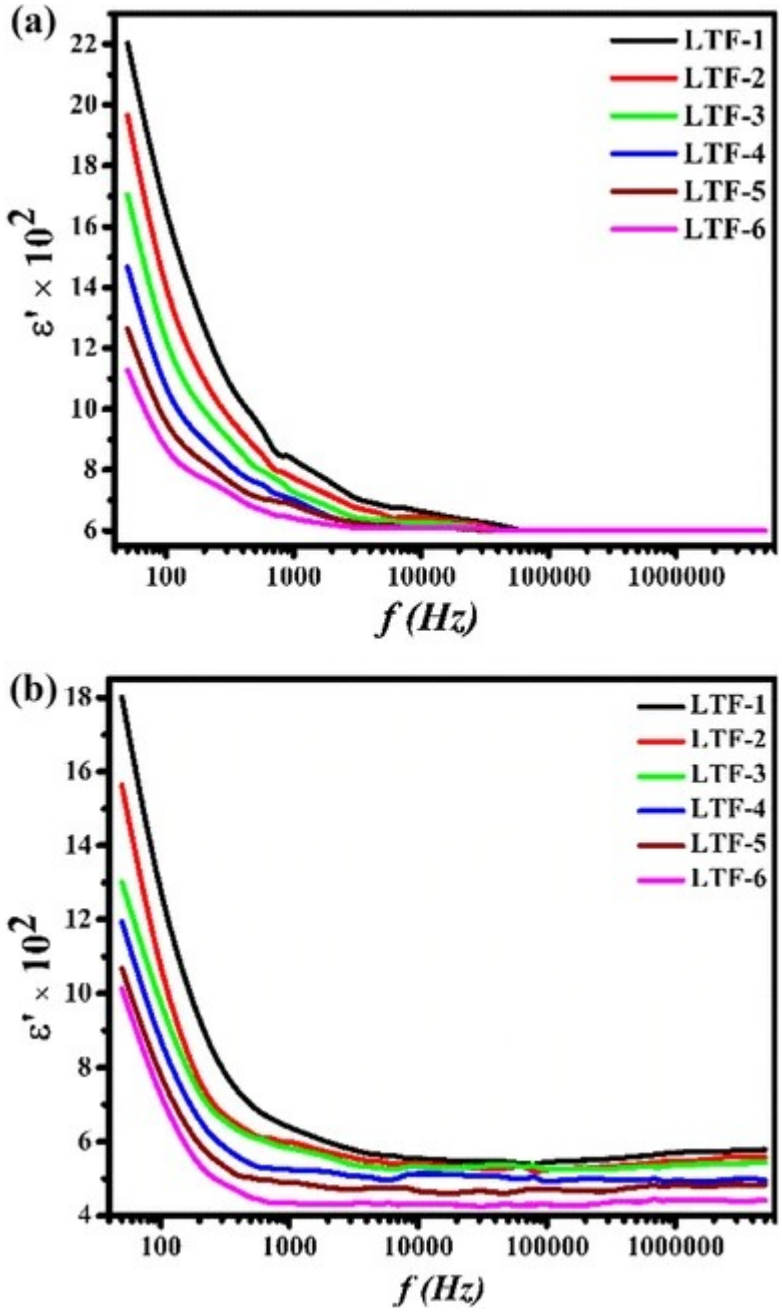

Frequency dependence of dielectric constant for a unirradiated and b γ-irradiated $Li_{0.5+0.5x}Ti_xFe_{2.5-1.5x}O_4$ nanoparticles. (Color figure online)

Fig. 12

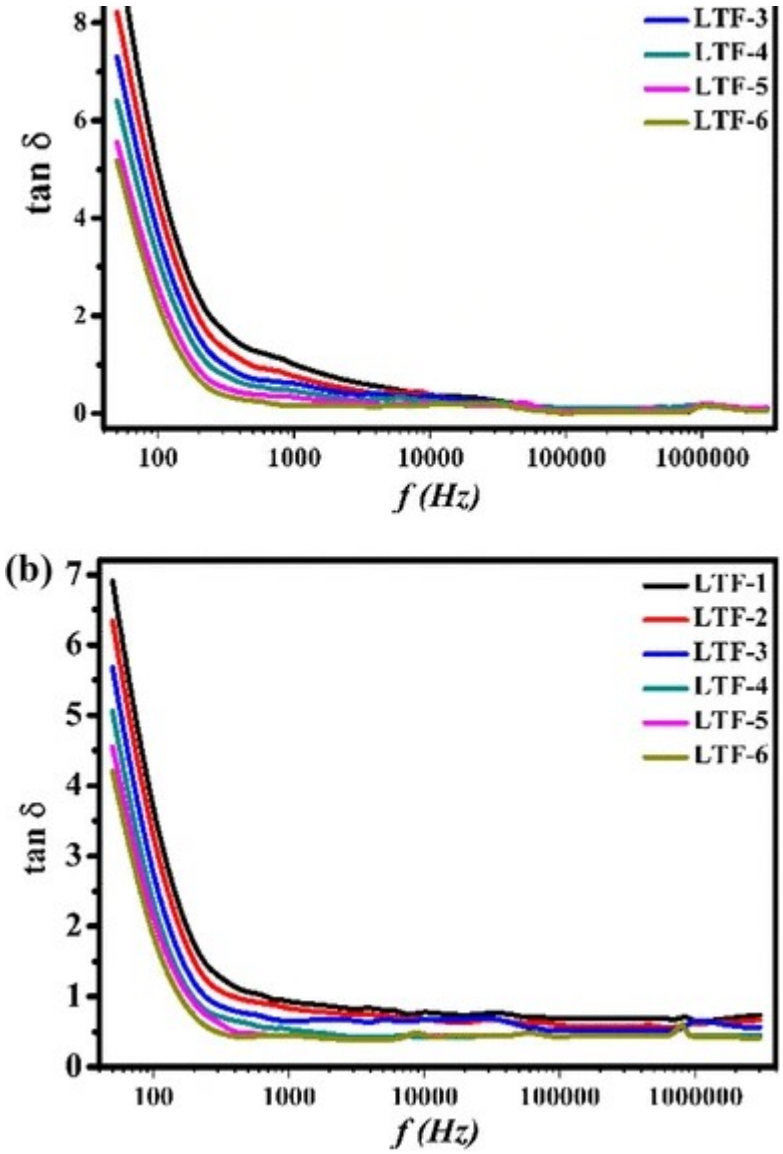

Frequency dependence of dielectric loss tangent for a unirradiated and b γ-irradiated $Li_{0.5+0.5x}Ti_xFe_{2.5-1.5x}O_4$ nanoparticles. (Color figure online)

It is observed from the behavior of dielectric loss tangent with frequency for all the samples shows exponentially decreasing tendency with an increase in frequency. Also, the values follow the same action, as observed in case of dielectric loss. The obtained results are in good agreement with the literature reports for Li-ferrite [18]. The impurity phases in LTF-5 and 6 (Figs. 5, 6) also affects the dielectric properties and from Figs. 11, 12 it is clear that the decrease rate in this parameters slows down.

4 Conclusion

The successful synthesis of Ti^{4+} ion substituted Li-ferrite achieved via sol–gel auto-combustion technique. XRD analysis revealed the single phase cubic spinel structure of the synthesized samples wherein the ordered-disorder transition observed after Ti^{4+} ion substitution for pristine and irradiated samples. The irradiated samples are more crystalline as compared with pristine. The lattice parameter for irradiated and pristine samples was found to be comparable with the JCPDS data for Li-ferrite and the crystallite size radically decrease after irradiation. FE-SEM images showed nano-sized spherical morphology for pristine samples whereas after irradiation the cracked morphology with nanosized grains was observed. The substitution of Ti^{4+} ions, as well as γ-radiation, greatly influenced the electrical and dielectric properties of Li-ferrites. DC resistivity increase with Ti^{4+} ion substitution, the room temperature dielectric properties of the system as a function of frequency showed the normal dispersion behavior and the values were found to be lower as compared to that for Li-ferrite after Ti^{4+} ions substitution. The irradiation causes a decrease in dielectric parameters and increases in DC resistivity. Overall the 5 Mrad γ-radiation dose can alter the structural, electrical and dielectric properties of Ti^{4+} ions substituted Li-ferrite, which gives better crystallinity, increase in DC resistivity and a decrease in dielectric properties.

References

1. A.V. Humbe, J.S. Kounsalye, M.V. Shisode, K.M. Jadhav, Ceram. Int. 44, 5466 (2018). https://doi.org/10.1016/j.ceramint.2017.12.180

Article CAS Google Scholar

2. A.V. Humbe, A.C. Nawle, A. Shinde, K. Jadhav, J. Alloys Compd. 691, 343 (2017)

Article CAS Google Scholar

3. H.M. Widatallah, C. Johnson, A.M. Gismelseed et al., J. Phys. D 41, 165006 (2008)

Article Google Scholar

4. P. Naderi, S.M. Masoudpanah, S. Alamolhoda, Appl. Phys. A 123, 702 (2017). https://doi.org/10.1007/s00339-017-1304-8

Article CAS Google Scholar

5. Y. Abbas, A.H. Ibrahim, Am. J. Mater. Sci. 4, 84 (2014)

Google Scholar

6. S. Soreto, M. Graça, M. Valente, L. Costa, in *Magnetic Spinels—Synthesis, Properties and Applications*, ed. by M.S. Seehra (InTech, Rijeka, 2017)

Google Scholar

7. N. Rezlescu, C. Doroftei, E. Rezlescu, P.D. Popa, Sens. Actuators B 133, 420 (2008). https://doi.org/10.1016/j.snb.2008.02.047

Article CAS Google Scholar

8. V. Sankaranarayanan, O. Prakash, R. Pant, M. Islam, J. Magn. Magn. Mater. 252, 7 (2002)

Article CAS Google Scholar

9. T. Collins, A. Brown, J. Appl. Phys. 42, 3451 (1971)

Article CAS Google Scholar

10. H. Zeng, T. Tao, Y. Wu et al., RSC Adv. 4, 23145 (2014). https://doi.org/10.1039/C4RA02957G

Article CAS Google Scholar

11. M.A. Dar, J. Shah, W.A. Siddiqui, R.K. Kotnala, J. Alloys Compd. 523, 36 (2012). https://doi.org/10.1016/j.jallcom.2012.01.083

Article CAS Google Scholar

12. M. Srivastava, A.K. Ojha, S. Chaubey, P.K. Sharma, A.C. Pandey, Mater. Sci. Eng. B 175, 14 (2010). https://doi.org/10.1016/j.mseb.2010.06.005

Article CAS Google Scholar

13. S. Misra, Mater. Res. Bull. 91, 203 (2017)

Article CAS Google Scholar

14. R.P. Patil, P.P. Hankare, K.M. Garadkar, R. Sasikala, J. Alloys Compd. 523, 66 (2012). https://doi.org/10.1016/j.jallcom.2012.01.025

Article CAS Google Scholar

15. B. Randhawa, H. Dosanjh, N. Kumar, J. Radioanal. Nucl. Chem. 274, 581 (2007)

Article CAS Google Scholar

16. L. Klein, M. Aparicio, A Jitianu (eds.), *Handbook of Sol-Gel Science and Technology* (Springer, Basel, 2017)

Google Scholar

17. S.S. Deshmukh, A.V. Humbe, A. Kumar, R.G. Dorik, K.M. Jadhav, J. Alloys Compd. 704, 227 (2017)

Article CAS Google Scholar

18. M.L. Mane, V.N. Dhage, K. Ranganathan, S.M. Oak, K.M. Jadhav, Radiat. Eff. Defects Solids 166, 435 (2011)

Article CAS Google Scholar

19. M.L. Mane, S.E. Shirsath, V.N. Dhage, K.M. Jadhav, Nucl. Instrum. Methods Phys. Res. B 269, 2026 (2011)

Article CAS Google Scholar

20. V.J. Deshmukh, P.S. Jadhav, K.K. Patankar, S.S. Suryawanshi, V.R. Puri, New J. Glass Ceram. 2, 122 (2012)

Article CAS Google Scholar

21. A. Farea, S. Kumar, K.M. Batoo, A. Yousef, C.G. Lee, J. Alloys Compd. 469, 451 (2009)

Article CAS Google Scholar

22. O. Hemeda, M. El-Saadawy, J. Magn. Magn. Mater. 256, 63 (2003)

Article CAS Google Scholar

23. A.V. Raut, D.V. Kurmude, D.R. Shengule, K.M. Jadhav, Mater. Res. Bull. 63, 123 (2015)

Article CAS Google Scholar

24. A. Karim, S.E. Shirsath, S.J. Shukla, K.M. Jadhav, Nucl. Instrum. Methods Phys. Res. B 268, 2706 (2010). https://doi.org/10.1016/j.nimb.2010.05.058

Article CAS Google Scholar

25. H. Hassan, T. Sharshar, M. Hessien, O. Hemeda, Nucl. Instrum. Methods Phys. Res. B 304, 72 (2013)

Article CAS Google Scholar

26. P.P. Naik, R.B. Tangsali, S.S. Meena, P. Bhatt, B. Sonaye, S. Sugur, Radiat. Phys. Chem. 102, 147 (2014). https://doi.org/10.1016/j.radphyschem.2014.04.038

Article CAS Google Scholar

27. J.S. Kounsalye, P.B. Kharat, M.V. Shisode, K.M. Jadhav JMSE (2017). https://doi.org/10.1007/s10854-017-7656-1

Article Google Scholar

28. R.D. Shannon, (1976) Acta Crystallogr. A 32, 751

Article Google Scholar

29. Z. Jian, W. Hejing, Chin. J. Geochem. 22, 38 (2003). https://doi.org/10.1007/bf02831544

Article Google Scholar

30. H.S.C. O'Neill, A. Navrotsky, Am. Miner. 68: 181 (1983)

Google Scholar

31. P. Coppens, *X-ray Charge Densities and Chemical Bonding* (IUCr, Oxford, 1997)

Google Scholar

32. A. Humbe, J. Kounsalye, M.V. Shisode, K.M. Jadhav, (2017) Rietveld Refinement, Morphology and Superparamagnetism of Nanocrystalline Ni 0.70−x Cu. x Zn 0.30 Fe 2 O 4 Spinel Ferrite

33. S. Saafan, S. Assar, B. Moharram, M.El Nimr, J. Magn. Magn. Mater. 322, 628 (2010)

Article CAS Google Scholar

34. K. El-Sayed, M.B. Mohamed, S. Hamdy, S.S. Ata-Allah, J. Magn. Magn. Mater. 423, 291 (2017). https://doi.org/10.1016/j.jmmm.2016.09.100

Article CAS Google Scholar

35. S.S. More, R.H. Kadam, A.B. Kadam, D.R. Mane, G.K. Bichile, Open Chem. 8, 419 (2010)

Article CAS Google Scholar

36. A.T. Raghavender, K.M. Jadhav, Int. J. Mod. Phys. B 23, 223 (2009)

Article CAS Google Scholar

37. R.D. Shannon, Acta Crystallogr. A 32, 751 (1976)

Article Google Scholar

38. V. Vinayak, P.P. Khirade, S.D. Birajdar, D.B. Sable, K.M. Jadhav, JOSC 29, 1025 (2016)

CAS Google Scholar

39. J.S. Kounsalye, A.V. Humbe, P.P. Khirade, A.R. Chavan, K. Jadhav, in *AIP Conference Proceedings* (AIP Publishing, New York, 2017)

40. C.M. Hurd, Contemp. Phys 23, 469 (1982)

Article CAS Google Scholar

41. S.R. Nimbore, D.R. Shengule, S.J. Shukla, G.K. Bichile, K.M. Jadhav, J. Mater. Sci. 41, 6460 (2006). https://doi.org/10.1007/s10853-006-0365-4

Article CAS Google Scholar

42. V.S. Sawant, A.A. Bagade, K.Y. Rajpure, Phys. B 474, 47 (2015). https://doi.org/10.1016/j.physb.2015.06.005

Article CAS Google Scholar

43. Y. Subramanian, S. Prakriteswar, J. Phys. Chem. 97, 3849 (1993)

Article Google Scholar

44. M.M. Eltabey, I.A. Ali, H.E. Hassan, M.N.H. Comsan, J. Mater. Sci. 46, 2294 (2011). https://doi.org/10.1007/s10853-010-5071-6

Article CAS Google Scholar

45. F. Kremer, A. Schönhals, *Broadband Dielectric Spectroscopy* (Springer, Berlin, 2012)

Google Scholar

46. C. Koops, Phys. Rev. 83: 121 (1951)

Article CAS Google Scholar

47. K. Iwauchi, Jpn. J. Appl. Phys. 10, 1520 (1971)

Article CAS Google Scholar

48. G.H. Kale, A.V. Humbe, D. Shankar, A. Birajdar, K. Shinde, Jadhav, J. Mater. Sci.: Mater. Electron. 27, 2151 (2016)

CAS Google Scholar

49. B.M. Sahanashree, E. Melagiriyappa, M. Veena et al., Radiat. Phys. Chem. 139, 55 (2017). https://doi.org/10.1016/j.radphyschem.2017.05.020

Article CAS Google Scholar

Acknowledgements

One of the authors (JSK) is thankful to 'The Government Institute of science, Aurangabad, Maharashtra (India)' for providing gamma radiation facility.

Author information

Authors and Affiliations

Department of Physics, Dr. Babasaheb Ambedkar Marathwada University, Aurangabad, M.S., India

Jitendra S. Kounsalye, Prashant B. Kharat, Dhananjay N. Bhoyar & K. M. Jadhav

Corresponding author

Correspondence to K. M. Jadhav.

Rights and permissions

About this article

Cite this article

Kounsalye, J.S., Kharat, P.B., Bhoyar, D.N. *et al.* Radiation-induced modifications in structural, electrical and dielectric properties of Ti^{4+} ions substituted $Li_{0.5}Fe_{2.5}O_4$ nanoparticles. *J Mater Sci: Mater Electron* 29, 8601–8609 (2018). https://doi.org/10.1007/s10854-018-8874-x

Received	Accepted	Published
12 January 2018	08 March 2018	13 March 2018

Issue Date
May 2018

DOI
https://doi.org/10.1007/s10854-018-8874-x

Share this article